analytical chemistry

Article

pubs.acs.org/ac

Enrichment of Cations via Bipolar Electrode Focusing

Eoin Sheridan,[†,§] Dzmitry Hlushkou,[‡] Kyle N. Knust,[†] Ulrich Tallarek,*[,‡] and Richard M. Crooks*[,†]

[†]Department of Chemistry and Biochemistry, Center for Electrochemistry, and the Center for Nano- and Molecular Science and Technology, The University of Texas at Austin, 1 University Station, A5300, Austin, Texas 78712-0165, United States

[‡]Department of Chemistry, Philipps-Universität Marburg, Hans-Meerwein-Strasse, 35032 Marburg, Germany

Supporting Information

ABSTRACT: We have previously demonstrated up to 5 × 10^5-fold enrichment of anionic analytes in a microchannel using a technique called bipolar electrode focusing (BEF). Here, we demonstrate that BEF can also be used to enrich a cationic fluorescent tracer. The important point is that chemical modification of the microchannel walls enables reversal of the electroosmotic flow (EOF), enabling cations, instead of anions, to be enriched via an electric field gradient focusing mechanism. Reversal of the EOF has significant consequences on the formation and shape of the region of the buffer solution depleted of charge carriers (depletion zone). Electric field measurements and numerical simulations are used to elucidate the factors influencing the depletion zone. This information is used to understand and control the location and shape of the depletion zone, which in turn influences the stability and concentration of the enriched band.

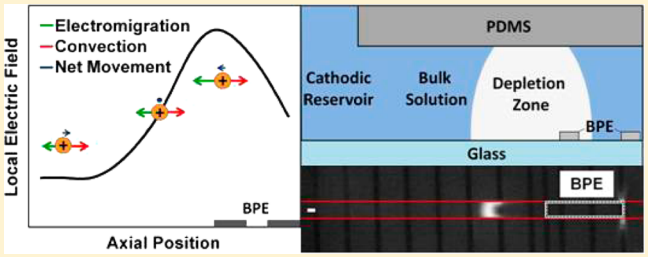

We have previously demonstrated up to 5 × 10^5-fold enrichment of anionic analytes in a microchannel using a technique called bipolar electrode focusing (BEF).[1] Here, we demonstrate that BEF can also be used to enrich cations. The important point is that chemical modification of the microchannel walls enables reversal of the electroosmotic flow (EOF), enabling cations, instead of anions, to be enriched via an electric field gradient focusing (EFGF) mechanism. Cation enrichment is enabled by either indirect buffer cation neutralization or indirect buffer anion neutralization, and here, we use numerical simulations and electric field measurements to reveal the mechanistic details for both. Our findings provide important insights into the dynamics of depletion zone formation in BEF and in all EFGF techniques employing a depletion zone for their function.

BEF is a versatile method being developed by our groups for analyte enrichment and separation.[1−7] In BEF, the local electric field within an electrolyte solution is manipulated in the vicinity of a bipolar electrode (BPE).[2−6] In brief, application of a voltage (E_{tot}) across a buffer-filled microchannel of length $l_{channel}$ results in an electric field having a constant value of $\sim E_{tot}/l_{channel}$. If a BPE is present in the microchannel (Scheme 1a,b) and if E_{tot} is sufficiently large, faradaic electrochemical reactions will occur at the two poles of the BPE (Scheme 1c). This situation is satisfied when the fraction of E_{tot} dropped over the length of the BPE ($\Delta E_{elec} = \sim E_{tot} \times (l_{elec}/l_{channel})$, where l_{elec} is the length of the BPE) exceeds that required to drive a reduction reaction at the cathodic pole and an oxidation at the anodic pole.[2−6] The key point is that the interfacial potential between the poles of the BPE and the solution is determined by E_{tot}, whereas the potential of the BPE floats to a constant potential.

Electrochemical processes may result in substantial changes to the ionic strength of the electrolyte near the BPE. For example, in the experiments reported here, the buffers used are Tris and carbonate. Water reduction at the BPE cathode generates OH^- (eq 1), which neutralizes $TrisH^+$ (eq 2). Likewise, water oxidation at the BPE anode (eq 3) leads to H^+, which neutralizes carbonate (eqs 4 and 5), thereby depleting charge carriers in solution and creating an electric field gradient near the poles of the BPE.

$$2H_2O + 2e^- \leftrightarrow H_2 + 2OH^- \quad (1)$$

$$TrisH^+ + OH^- \leftrightarrow Tris + H_2O \quad (2)$$

$$2H_2O - 4e^- \leftrightarrow O_2 + 4H^+ \quad (3)$$

$$2H^+ + CO_3^{2-} \leftrightarrow H_2O + CO_2 \quad (4)$$

$$H^+ + HCO_3^- \leftrightarrow H_2O + CO_2 \quad (5)$$

Additional information about the reactions occurring in the microchannel is provided in the Supporting Information. We have previously shown that anions can be enriched in the presence of an electric field gradient when the electrophoretic velocity, which depends on the local electric field strength, is equal in magnitude but opposite in direction to the electroosmotic velocity. The latter is nearly constant throughout the channel due to the incompressibility of water, but the former depends on the types of faradaic and homogeneous

Received: April 26, 2012
Accepted: August 1, 2012
Published: August 14, 2012

Scheme 1

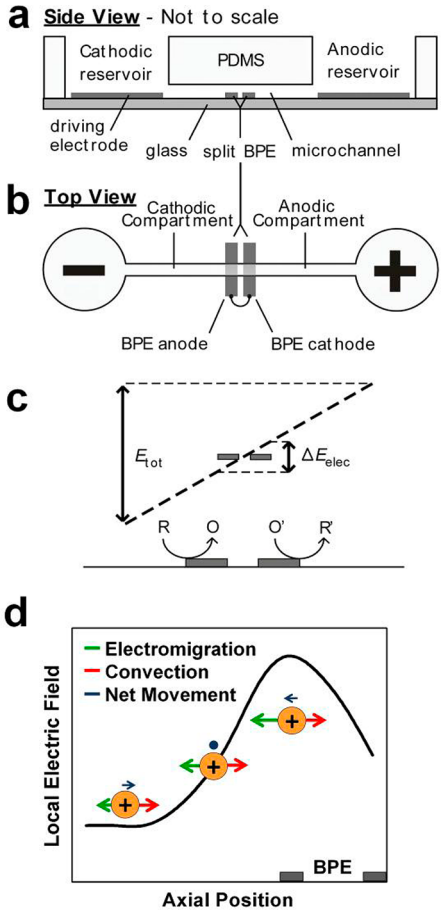

reactions represented by eqs 1−5.[1−6] Here, we show that cations can be enriched by reversing the EOF such that convection (dominated by electroosmosis) is opposite in direction to electromigration (EM) of the cations (Scheme 1d).

Microfluidic-based sensors having multiple integrated functions are now commonplace.[8−11] For example, due to the small number of molecules in such devices (low volumes and concentrations), it is often desirable to enrich the concentration of analytes. Many methods have been reported for accomplishing this task, including electrokinetic membrane filtration,[12,13] solid-phase extraction (SPE),[14,15] isoelectric focusing (IEF),[16−18] and temperature gradient focusing (TGF).[19,20] BEF is a form of EFGF, an approach for microfluidic concentration enrichment frequently used in chip-based analytical devices.[21−28] Enrichment factors (EFs) of up to 10^7 have been reported using other members of the EFGF family.[21] Until now, the vast majority of EFGF techniques have focused on anionic enrichment due to difficulties in producing a device capable of flowing EOF against the direction of cation EM using standard materials. One notable exception, reported by Ivory and co-workers, involved cation enrichment by application of reversed polarity potential profiles directly to the enrichment and separation channel. This technique is effective but requires some experimental overhead to remove the products of water electrolysis from the channel.[29]

In this work, we present a method for chemically reversing the direction of EOF within a microfluidic device such that cationic enrichment can be achieved. We illustrate the effectiveness of the method using the tracer cation tris(bipyridine)ruthenium(II) dichloride ($[Ru(bpy)_3]^{2+}$). The results show that reversal of the EOF has a significant influence on the way the depletion zone forms. Experimental measurements and simulations provide a context for understanding these phenomena and hence a basis for optimizing conditions to improve cation enrichment efficiency. For example, the use of carbonate buffer, which is neutralized by H^+ (rather than OH^-), leads to a compact and efficiently formed depletion zone and therefore more highly enriched cation concentrations and narrower enriched analyte bands.

EXPERIMENTAL SECTION

Chemicals. Poly(dimethylsiloxane) (PDMS) channels were prepared using a Sylgard 184 elastomer kit obtained from K. R. Anderson, Inc. (Morgan Hill, CA). Au-coated glass slides (100 nm thick, no adhesion layer) were purchased from EMF Corp. (Ithaca, NY). $[Ru(bpy)_3]^{2+}$ was purchased from Sigma-Aldrich (St. Louis, MO). Tris buffer (pH 8.1) was prepared by dilution of a 1.0 M Tris−HCl solution purchased from Fisher (Fair Lawn, NJ). A 0.5 M stock solution of carbonate buffer (pH 10.0) was prepared from 99% sodium bicarbonate (Sigma-Aldrich, St. Louis, MO) by dissolution in deionized water and titration with 1.0 M NaOH solution (EMD Chemicals, Gibbstown, NJ). This stock solution was then diluted to 1.0 mM (pH 10.0) and used as background electrolyte. Photoresist (AZ 4620) and developer (AZ 421 K) were purchased from AZ Electronic Materials (Somerville, NJ). Hexadimethrine bromide (Polybrene) and Rhodamine B were purchased from Sigma-Aldrich. All chemicals were used as received. Deionized (DI) water having a resistivity of 18.2 MΩ·cm was used for all experiments (Milli-Q gradient system, Millipore, Bedford, MA).

Microfluidic Device Fabrication. Device fabrication has been described previously.[2,3] Briefly, the driving electrodes and BPEs were deposited onto the glass base of the microfluidic device using standard photolithographic techniques. The driving electrodes consisted of microfabricated Au disks located at the bottoms of the two reservoirs. They were connected to a power supply via external contacts. An array of 16 gold microband electrodes consisting of 30 μm-wide lines and 70 μm-wide spaces was used to form split BPEs and to measure the electric field gradient. The microbands had external contacts so that any two could be connected to form a BPE or to measure the solution potential in the microchannel.

Microchannels were fabricated in PDMS using a previously described replica molding procedure.[3,30] Briefly, a microfluidic channel (6 mm long, 100 μm wide, and 21 μm high) spanning two 5.0 mm-diameter reservoirs was fabricated from PDMS. The PDMS was rinsed with ethanol and dried under N_2, and then, both the PDMS and the glass slide supporting the Au electrodes were exposed to an O_2 plasma (60 W, model PDC-32G, Harrick Scientific, Ossining, NY) for 30 s on the medium power setting. After joining the PDMS replica and the glass slide, the entire assembly was placed in an oven at 65 °C for 5 min to promote irreversible bonding.

Modification of the channel walls with a Polybrene monolayer was carried out as follows. The microfluidic device was loaded with a 3.0 μM Polybrene solution and allowed to equilibrate for 20 h at 23 ± 2 °C, and then, the channel was thoroughly rinsed with water and used immediately without further treatment. Polybrene forms an electrostatically adsorbed monolayer on the microchannel walls. Polybrene is positively charged at the pH used in the experiments reported here, and therefore, it reverses the direction of EOF in microchannels.[31]

dx.doi.org/10.1021/ac301101b | Anal. Chem. 2012, 84, 7393−7399

Instrumentation and Data Acquisition. Fluorescence images were obtained using a Nikon AZ100 (Nikon Co., Tokyo, Japan) microscope equipped with a mercury lamp (Nikon) and a CCD camera (Cascade, Photometrics Ltd., Tucson, AZ). Micrographs were processed using V++ Precision Digital Imaging software (Digital Optics, Auckland, New Zealand). Images were captured using 1 × 1 binning with 512 × 290 pixels and a 100 ms exposure time. Fluorescence intensities for calibration curves were obtained using a function that averages intensities of all pixels along one axis of the region of interest. Fluorescence intensities of concentrated analyte bands were obtained using a maximum function in the software, which provides the maximum fluorescent intensity value within a region of interest (corresponding to the point at which enrichment is greatest in the concentrated band). The EF was calculated by dividing the maximum concentration in the enriched tracer band by the initial tracer concentration. Absolute concentrations of the enriched bands were determined by comparing the region of maximum intensity in the concentrated band of dye to calibrated fluorescence intensities.

Concentration Enrichment Experiments. Prior to each enrichment experiment, the microfluidic channel was rinsed by introducing 80.0 μL of sample solution (1.0−10.0 μM $[Ru(bpy)_3]^{2+}$ in either 5.0 mM Tris buffer (pH 8.1) or 1.0 mM carbonate buffer (pH 10.0)) into the anodic reservoir and 15.0 μL into the cathodic reservoir. The sample solution was allowed to flow through the microchannel for 20 min in response to the solution height differential. Next, the sample solution in both reservoirs was removed and replaced with equal 80.0 μL volumes of sample solution. To enhance the stability of the depletion zone during enrichment, pressure driven flow (PDF) was introduced by adding additional volumes of sample solution to the reservoirs. The specifics of this process are discussed in the Results and Discussion section, but the important point is that PDF may enhance or suppress convection resulting from electroosmosis.

The concentration enrichment experiments themselves were carried out as follows. First, two microband electrodes having the desired separation (typically 500 μm) were connected using a conductive wire. Second, a driving voltage (E_{tot} = 30.0−60.0 V) was applied across the microchannel using a high-voltage power supply (LLS9120, TDK-Lambda Americas, Inc., San Diego, CA) connected to the microfabricated gold driving electrodes spanning the bottoms of the reservoirs. The PDF rate in the microchannel was estimated after each experiment by switching off E_{tot} and observing the movement of the enriched band under the influence of PDF only. EOF mobility (μ_{EOF}) was measured by loading a 1.0 M solution of Rhodamine B (neutral) into one of the reservoirs and DI water into the other under conditions of zero PDF. A potential was applied, and the time required for the Rhodamine B front to traverse the microchannel via EOF was recorded using the fluorescence microscope.

Electric Field Profile Measurements. The axial electric field profile within the channel was monitored using a scanning digital multimeter (SDMM, Model 2700, Keithley Instruments, Inc., Cleveland, OH) equipped with a multiplexer module (Model 7701, Keithley) connected to all the microband electrodes except those defining the BPE. The SDMM was controlled with Microsoft Excel via the software provided by the SDMM manufacturer (ExceLinx, Keithley). The SDMM was interfaced to the microband electrodes through a breakout board (screw terminals). The SDMM sequentially reads the voltage difference between pairs of microbands. The acquisition time for each voltage measurement was ∼0.1 s, and the voltage between pairs of microbands was read every 2.0 s. Electric field monitoring experiments proceeded as follows. First, the two halves of the BPE were connected via a conductive wire. Second, the SDMM was placed into scan mode. Third, a driving voltage (E_{tot} = 30.0−60.0 V) was applied across the microchannel via the driving electrodes. The captured data were stored and plotted (Microsoft Excel) in real time as voltage differences between each microband pair vs time.

Computer Simulations. The spatiotemporal fields representing the state of the modeled system are defined by the species concentration and the electric potential distributions. The local species concentrations are governed by the Nernst−Planck equations:

$$\frac{\partial c_i}{\partial t} = D_i\left(\nabla^2 c_i + c_i\frac{z_i F}{RT}\nabla^2\varphi\right) - c_i\nabla\cdot\mathbf{v} + r_i \tag{6}$$

where c_i is the molar concentration of species i, D_i and z_i are its diffusion coefficient and valency, respectively, φ is the local electric potential; F, R, and T represent the Faraday constant, molar gas constant, and temperature, respectively, $\mathbf{v}$ is the flow velocity, and r_i is the reaction rate for species i (mol/s). Equation 6 describes local changes in species concentrations due to diffusion, EM, and advection as well as those arising from volume (chemical) and surface (faradaic) reactions.

The local concentrations of the charged species and the local electric potential are related by the Poisson equation:

$$-\varepsilon_0\varepsilon_r\nabla^2\varphi = 10^3 F\sum_i z_i c_i \tag{7}$$

where ε_0 and ε_r are the vacuum permittivity and dielectric constant of the electrolyte solution. The right side of eq 7 represents the local volume charge density expressed in terms of the species molar concentrations. Further, assuming the liquid to be incompressible, the generalized Navier−Stokes equation establishes the relationship between the local flow velocity, hydrostatic pressure p, and the body force due to the electrostatic interactions (the Lorentz force):

$$\rho\left(\frac{\partial\mathbf{v}}{\partial t} + \mathbf{v}\cdot\nabla\mathbf{v}\right) = -\nabla p + \mu\nabla^2\mathbf{v} - 10^3 F\nabla\varphi\sum_i z_i c_i \tag{8}$$

where ρ and μ are the mass density and dynamic viscosity of the liquid. Details of the reactions occurring within the microchannel and their rate constants are given in the Supporting Information.

All numerical schemes were realized as parallel codes in the C language using the Message Passing Interface (MPI) standard. The computational model was implemented at a supercomputer (SGI Altix 4700) of the "Leibniz-Rechenzentrum der Bayerischen Akademie der Wissenschaften" (Garching, Germany). A typical simulation to analyze the temporal behavior of the system for 100 s required ∼8 h at 128 processor cores and around 20 GB of system memory. More details of the computational model are given in the Supporting Information.

RESULTS AND DISCUSSION

Reversing the Direction of Electroosmosis. To achieve enrichment of ions via an EFGF mechanism, it is necessary to balance two opposing forces. Because cationic EM must be toward the direction of the cathodic reservoir, it is necessary

dx.doi.org/10.1021/ac301101b | Anal. Chem. 2012, 84, 7393−7399

that convection (which is dominated by EOF) be toward the anodic reservoir. However, the native net charge on the microchannel walls, consisting of PDMS and glass, is negative,[32] which results in EOF toward the cathodic reservoir. Therefore, it is necessary to coat the microchannel walls with a positively charged polymer, which has previously been shown to reverse the direction of the EOF in related systems.[33] Here, the microchannel walls were coated with cationic Polybrene by loading the channel with a 3.0 μM solution for 20 h prior to the experiment. The microchannel was then rinsed with DI water to remove Polybrene not bound to the microchannel surface. The measured electroosmotic mobility (μ_{EOF}) in the modified microchannel was 2.42×10^{-8} m^2/(V s) (in 5.0 mM Tris buffer) and 2.84×10^{-8} m^2/(V s) (in 1.0 mM carbonate buffer), and in both cases, the EOF was in the direction of the anodic reservoir.

Cationic Enrichment in Tris−HCl Buffered Solution. We have previously demonstrated enrichment of anions by BEF using a Tris−HCl buffer solution.[2,3] In these experiments, TrisH$^+$ is neutralized by the products of water reduction according to eqs 1 and 2. The neutralization reaction at the BPE results in the formation of an ion depletion zone and subsequent local enrichment in the vicinity of the electric field gradient.

Figure 1 shows that $[Ru(bpy)_3]^{2+}$ can be enriched in a Polybrene-coated microchannel and that enrichment occurs in the anodic compartment between the BPE and the anodic reservoir. This experiment was carried out as follows. First, the microchannel surface was coated with Polybrene, as described in the Experimental Section, to reverse the EOF. Second, the microchannel was filled with 10.0 μM $[Ru(bpy)_3]^{2+}$ in 5.0 mM TrisH$^+$ buffer. Third, E_{tot} = 60.0 V was applied across the microchannel. Fourth, the PDF was adjusted until enrichment was initiated (30 μm/s toward the anode in this case). A slightly enriched band was visible near the BPE after just a few seconds. Over time, this band became more intense and slowly drifted toward the anodic reservoir (Figure 1, t = 60 s). As enrichment proceeds, the shape of the band changed (Figure 1, t = 120 s), and it continued to drift further from the BPE. This behavior continued until t = 300 s, shortly after which the enriched band drifted into the anodic reservoir and the experiment was terminated. Note that there is some mild discoloration evident on some of the microbands present in the center of the microchannel in Figure 1 (at all times during the experiment). This resulted from an earlier experiment in the same microchannel during which $[Ru(bpy)_3]^{2+}$ was oxidized on the microband surface. The discoloration, which is picked up by the fluorescent filter, did not influence the performance of the microbands and does not indicate enrichment at that location.

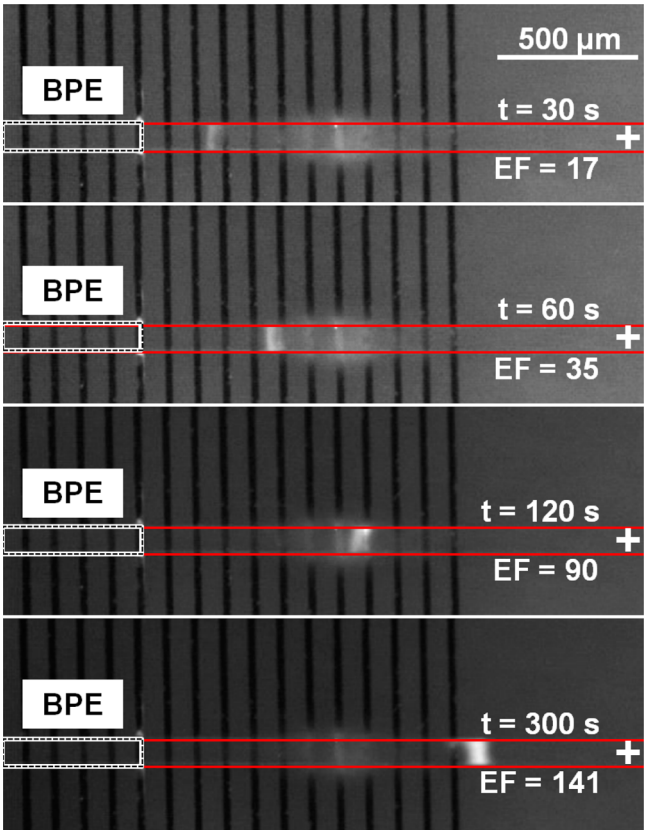

Figure 1. Fluorescence micrographs showing enrichment of $[Ru(bpy)_3]^{2+}$. The initial concentrations in the 6.0 mm-long microchannel were 5.0 mM Tris−HCl (pH 8.1) and 10.0 μM $[Ru(bpy)_3]^{2+}$, and the BPE had a length of 500 μm. The enrichment factors (EFs) are given in the images. E_{tot} = 60.0 V.

The results of this experiment are qualitatively similar to the case of anionic enrichment in Tris buffer,[3,34] but there are also some significant quantitative differences. For example, under identical conditions (except in an uncoated microchannel), enrichment of an anionic tracer, BODIPY^{2-}, commences at a significantly lower applied voltage (E_{tot} = 25.0 V),[6] compared to $[Ru(bpy)_3]^{2+}$ (E_{tot} = 60.0 V). This suggests that formation of the depletion zone is less efficient for cationic enrichment. The correspondingly higher E_{tot} required for cationic enrichment leads to bubble formation, arising from the generation of O_2 and H_2 gases at the BPE (eqs 1 and 3), which leads to less stable enrichment. This latter point is evident from the data in Figure 1, where the enriched $[Ru(bpy)_3]^{2+}$ band has an ill-defined shape and eventually drifts into the anodic reservoir. In contrast, anionic enrichment can be carried out for t > 2 h, and the band maintains a nearly constant shape and position within the microchannel.[34]

The EFs (defined in the Experimental Section) corresponding to the bands shown in Figure 1 are 17-fold (30 s), 35-fold (60 s), 90-fold (120 s), and 141-fold (300 s). These EFs are similar to those reported for anionic enrichment in similar experiments in uncoated microchannels; for example, ∼100-fold after 300 s using a lower E_{tot} = 35.0 V.[34] We conclude that the nature of cationic enrichment in Tris buffer is analogous to that of anionic enrichment, with the main difference being the need for a higher value of E_{tot} and the corresponding difficulties associated with faradaic reactions at the BPE.

To better understand the reasons underpinning the need for a higher value of E_{tot} for cationic enrichment (compared to anionic enrichment) in Tris buffer, we measured the electric field profile in a microchannel during enrichment. Figure 2a shows an electric field profile measured in the anodic compartment during the experiment represented in Figure 1. The microband electrodes visible to the right of the BPE in Figure 1 were used for this purpose. The results show that an electric field gradient forms, corresponding to an ion depletion zone. However, the gradient is rather shallow (ΔV = ∼3 kV/m) compared to previously reported gradients for anionic enrichment (ΔV = ∼7 kV/m),[6] suggesting a relatively small change in TrisH$^+$ concentration near the BPE. This conclusion is confirmed by the simulated TrisH$^+$ concentration profile

dx.doi.org/10.1021/ac301101b | Anal. Chem. 2012, 84, 7393−7399

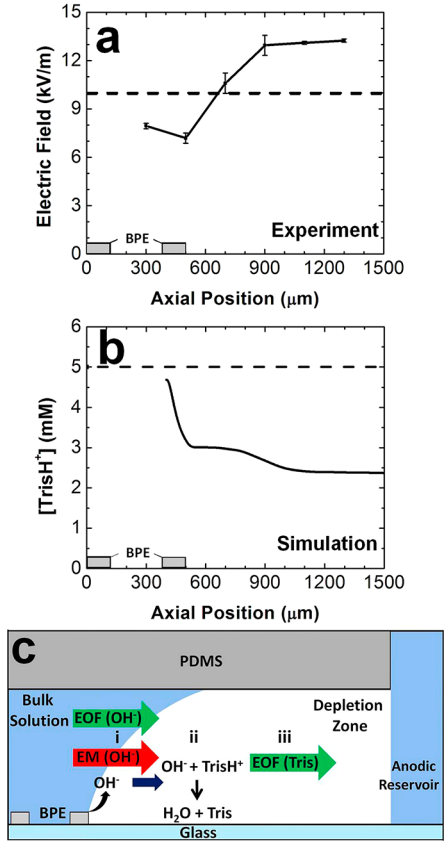

Figure 2. (a) Axial electric field profile measured during the enrichment experiment shown in Figure 1 (t = 300 s, solid line). The error bars indicate the standard deviation of three replicate measurements. The dashed line is an estimate of the electric field strength in the absence of a BPE. (b) Simulated $TrisH^+$ concentration profiles during the experiment shown in Figure 1 before enrichment (dashed line) and during enrichment (solid line). The initial concentrations in the 6.0 mm-long microchannel were 5.0 mM Tris–HCl (pH 8.1) and 10.0 μM $[Ru(bpy)_3]^{2+}$. The BPE was situated at axial position 0–500 μm. (c) Graphical representation (not to scale) of the microchannel (side-view, anodic compartment) showing the relevant chemical and electrochemical reactions as well as the evolution of the depletion zone.

(Figure 2b). The key point is that, with the EOF reversed, the $TrisH^+$ concentration is depleted to ~45% of its original value by the neutralization reaction (eq 2) in the depletion zone. Note that we have previously shown that $[TrisH^+]$ is less than 10% of its bulk value in the depletion zone during experiments wherein the EOF is not reversed.[6]

Like the experiments, the simulations reveal a broad depletion zone. These characteristics are a consequence of the direction of both the EM and EOF being toward the anodic reservoir (Figure 2c(i)). This causes the neutralization reaction (eq 2) to occur within the anodic compartment (Figure 2c(ii)). Neutralized Tris continues to move toward the anodic reservoir by EOF after neutralization (Figure 2c(iii)). The result is a broad region partially depleted of $TrisH^+$ stretching from the BPE to the anodic reservoir, as shown in Figure 2b. Therefore, the reversal of EOF, while necessary to facilitate cationic enrichment, is detrimental to the enrichment efficiency because it stretches the depletion zone away from the BPE, thereby decreasing the slope of the electric field gradient. Importantly, we have shown previously that the magnitude of the EF, the width of the enriched band, and the speed of enrichment are all a function of the steepness of the electric field gradient.[34]

Cationic Enrichment in Carbonate Buffered Solution. As discussed in the last paragraph, it is not possible to form a compact depletion zone using $TrisH^+$ buffer. However, a judicious choice of buffer can circumvent this problem. Specifically, we chose to repeat these experiments using carbonate (CO_3^{2-}/HCO_3^-) buffer, because in this case, the neutralization reaction relies on generation of H^+ (rather than OH^-) in the cathodic compartment (rather than the anodic compartment) of the microchannel. The carbonate experiment was carried out as follows. First, a Polybrene-coated microchannel was filled with 10.0 μM $[Ru(bpy)_3]^{2+}$ in 1.0 mM (pH = 10.0) carbonate buffer. Next, E_{tot} = 30.0 V was applied across the microchannel. Then, the PDF was adjusted until enrichment could be observed by fluorescence microscopy. In this case, a PDF of 55 μm/s toward the cathode was applied. Note that the buffer concentration for the carbonate system (1.0 mM) is lower than for the Tris buffer (5.0 mM). The buffer concentrations were selected on the basis of experimental observation of the most stable enriched band at various buffer concentrations. Because the magnitude of the electric field gradient depends on the relative change in buffer ion concentration, the initial buffer concentration is not of special importance for a particular experiment.

The results of the carbonate enrichment experiment are shown in Figure 3. Here, a compact band of enriched

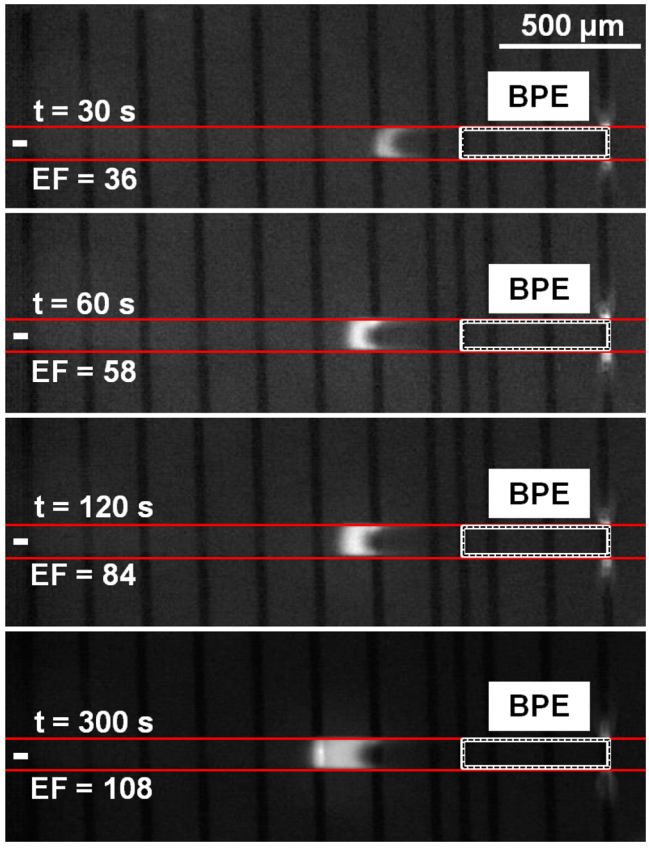

Figure 3. Fluorescence micrographs showing enrichment of $[Ru(bpy)_3]^{2+}$. The initial concentrations in the 6.0 mm-long microchannel were 1.0 mM carbonate buffer (pH 10.0) and 10.0 μM $[Ru(bpy)_3]^{2+}$, and the BPE had a length of 500 μm. The enrichment factors (EFs) are given in the images. E_{tot} = 30.0 V.

dx.doi.org/10.1021/ac301101b | Anal. Chem. 2012, 84, 7393–7399

$[Ru(bpy)_3]^{2+}$ forms within 20 s in the cathodic compartment of the microchannel. The EFs shown in the figure are similar to those reported for anionic enrichment in Tris using an uncoated microchannel having similar dimensions (EF = ~100 after 300 s).[34] Importantly, compared to the Tris system (Figure 1), the shape and position of the band are quite stable over the 300 s course of this experiment. The time-dependent band broadening apparent in Figure 3 is a consequence of the electric field gradient becoming more shallow as the experiment progresses. We have previously shown that this is intrinsic to the enrichment process.[34] That is, enrichment of ions within the depletion zone naturally leads to increased ion concentration in the depletion zone, and this results in a continuous reduction in the magnitude of the electric field gradient. This problem becomes serious when the concentrations of the buffer and enriched band approach each other. This means that BEF is most efficient for dilute concentrations of analytes, which of course is the exact situation when one would like to use this method.

In the just-described experiment, enrichment begins at E_{tot} = 30.0 V, which is significantly lower than is required for cationic enrichment in Tris buffer (60.0 V). The lower value of E_{tot} eliminates bubble formation at the BPE, and hence, it is responsible for both the stable shape and position of the enriched band compared to the Tris experiment. Greater stability means that enrichment can proceed for longer times (recall, when Tris buffer was used, the enriched band drifted into the anodic reservoir within ~300 s). This point is illustrated in Figure S1 (Supporting Information), where a 20 min enrichment experiment is shown. In this case, the initial concentration of the $[Ru(bpy)_3]^{2+}$ solution was 1.0 μM and the EF = 274. Presumably much lower concentrations could be enriched, but the detection limit of our optical system corresponds to 1.0 μM $[Ru(bpy)_3]^{2+}$. Note also that the enriched concentration, 0.274 mM, is, as discussed in the previous paragraph, on the order of the buffer concentration (1.0 mM). In contrast to these results obtained using carbonate buffer, it was not possible to enrich $[Ru(bpy)_3]^{2+}$ from initial concentrations <10.0 μM using Tris.

The electric field profile measured in the cathodic compartment during the experiment shown in Figure 3 is provided in Figure 4a. In this case, the electric field gradient is relatively steep (ΔV = ~8 kV/m) compared to the Tris system (ΔV = ~3 kV/m, Figure 2a), suggesting a greater change in buffer concentration near the BPE compared to the Tris buffer. This is confirmed by the simulated buffer concentration profiles shown in Figure 4b. The major contributor to ionic strength, CO_3^{2-}, was depleted to <25% of its initial concentration, compared to the $TrisH^+$ case, which remained at >45% of its initial concentration (Figure 2b). This more efficient distribution of charges in the microchannel accounts for the lower E_{tot} required to initiate cationic enrichment in carbonate buffer (30.0 V) compared to Tris buffer (60.0 V), as a greater proportion of E_{tot} is dropped in the high-resistance depletion zone.

The experimental results in Figure 4a also show that the region of elevated electric field strength is significantly more compact in the carbonate system, compared to that shown in Figure 2a for Tris indicating a more compact depletion zone. This observation is confirmed by the simulated carbonate buffer concentration profiles shown in Figure 4b. The more compact ion depletion zone arises because H^+ (formed at the BPE, eq 3) electromigrates opposite to the direction of the EOF (i.e.,

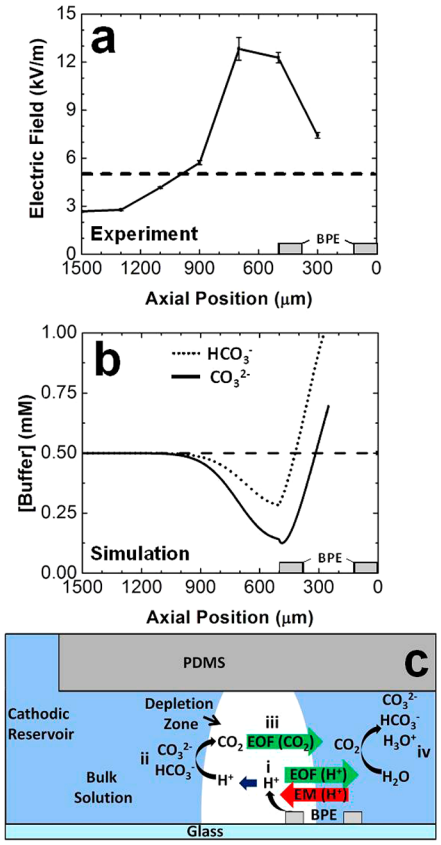

Figure 4. (a) Axial electric field profile measured during the enrichment experiment shown in Figure 3 (t = 300 s, solid line). The error bars indicate the standard deviation of three replicate measurements. The dashed line is an estimate of the electric field strength in the absence of a BPE. (b) Simulated CO_3^{2-} (solid line) and HCO_3^- (dotted line) concentration profiles during the experiment shown in Figure 3. The dashed line shows the concentration of both species before enrichment. The initial concentrations in the 6.0 mm long microchannel were 1.0 mM carbonate buffer (pH 10.0) and 10.0 μM $[Ru(bpy)_3]^{2+}$. The BPE was at axial position 0–500 μm. (c) Graphical representation (not to scale) of the microchannel (side-view, cathodic compartment) showing the relevant chemical and electrochemical reactions as well as the evolution of the depletion zone.

toward the cathodic compartment (Figure 4c(i)) until it reacts with CO_3^{2-} (eq 4) or HCO_3^- (eq 5) and is neutralized (Figure 4c(ii)). Neutral CO_2(aq) formed in the cathodic compartment moves toward the BPE anode via EOF (Figure 4c(iii)). This causes the depletion zone to be situated adjacent to the BPE anode and remain compact instead of spreading away from the BPE into the microchannel as shown in Figure 2c.

Notice that Figure 4b shows the concentrations of both CO_3^{2-} and HCO_3^- are higher than their initial values in the region of the channel above the BPE. This is caused by the excess of CO_2(aq) in the region between the BPE cathode and anode reacting with water to form carbonic acid, which subsequently dissociates into CO_3^{2-}, HCO_3^-, and H^+ (Figure 4c(iv)). This equilibrium further serves to enhance the compactness of the depletion zone by preventing it from stretching into the anodic compartment. A more compact ion depletion zone means the band position is more stable, enabling longer enrichment times and higher EFs.[34]

The key to optimizing the enrichment process is to ensure that the neutralization reaction occurs in the appropriate

dx.doi.org/10.1021/ac301101b | Anal. Chem. 2012, 84, 7393–7399

compartment and that the neutral reaction products move toward the BPE via EOF (Figure 4c). When neutralized products move away from the BPE (Figure 2c), the depletion zone spreads out across the length of the microchannel, which destabilize the electric field gradient. This same observation holds for enrichment of anions. In this case, the EOF must be in the direction of the cathode, and higher EFs arise using Tris buffer (neutralized by OH^-) rather than carbonate buffer (neutralized by H^+).[2]

SUMMARY AND CONCLUSIONS

The findings reported here improve our understanding of BEF and other EFGF techniques that rely on a compact, stable depletion zone. This in turn provides a basis for implementing interesting new separation and enrichment schemes. Although the EFs demonstrated in this work are modest, we have previously shown that anions can be enriched by nearly 1 million-fold using BEF.[1] There are two principal factors that limit the maximum attainable enrichment. First, the electric field gradient, which can be increased by reducing the dimensions of the channel and through the use of two channels configured with a bridging BPE. Second, the highest EFs are attained for low analyte concentrations. This is because enrichment stops when the analyte concentration in the enriched bands approaches that of the buffer. Finally, in a forthcoming publication, we will show that the principles reported in this paper can be used to simultaneously concentrate both anions and cations.[35]

ASSOCIATED CONTENT

Supporting Information

Additional information about the simulations and results for a 20 min experiment showing enrichment of $[Ru(bpy)_3]^{2+}$ from an initial concentration of 1.0 μM in carbonate buffer. This material is available free of charge via the Internet at http://pubs.acs.org.

AUTHOR INFORMATION

Corresponding Author

*E-mail: crooks@cm.utexas.edu (R.M.C.); tallarek@staff.uni-marburg.de (U.T.).

Present Address

[§]School of Mathematics and Physics, University of Queensland, Brisbane, St Lucia, Queensland 4072, Australia.

Notes

The authors declare no competing financial interest.

ACKNOWLEDGMENTS

This work was funded by the Division of Chemical Sciences, Geosciences, and Biosciences, Office of Basic Energy Sciences of the U.S. Department of Energy through Grant DE-FG02-06ER15758. We also thank the Robert A. Welch Foundation (Grant F-0032) for sustained support. Simulations were run at the "Leibniz-Rechenzentrum der Bayerischen Akademie der Wissenschaften" (Garching, Germany), supported by project HLRB pr26wo.

REFERENCES

(1) Anand, R. K.; Sheridan, E.; Knust, K. N.; Crooks, R. M. *Anal. Chem.* **2011**, *83*, 2351−2358.
(2) Laws, D. R.; Hlushkou, D.; Perdue, R. K.; Tallarek, U.; Crooks, R. M. *Anal. Chem.* **2009**, *81*, 8923−8929.
(3) Perdue, R. K.; Laws, D. R.; Hlushkou, D.; Tallarek, U.; Crooks, R. M. *Anal. Chem.* **2009**, *81*, 10149−10155.
(4) Dhopeshwarkar, R.; Hlushkou, D.; Nguyen, M.; Tallarek, U.; Crooks, R. M. *J. Am. Chem. Soc.* **2008**, *130*, 10480−10481.
(5) Hlushkou, D.; Perdue, R. K.; Dhopeshwarkar, R.; Crooks, R. M.; Tallarek, U. *Lab Chip* **2009**, *9*, 1903−1913.
(6) Sheridan, E.; Hlushkou, D.; Anand, R. K.; Laws, D. R.; Tallarek, U.; Crooks, R. M. *Anal. Chem.* **2011**, *83*, 6746−6753.
(7) Sheridan, E.; Knust, K. N.; Crooks, R. M. *Analyst* **2011**, *136*, 4134−4137.
(8) Du, Y.; Chen, C.; Zhou, M.; Dong, S.; Wang, E. *Anal. Chem.* **2011**, *83*, 1523−1529.
(9) Salehi-Reyhani, A.; Kaplinsky, J.; Burgin, E.; Novakova, M.; deMello, A. J.; Templer, R. H.; Parker, P.; Neil, M. A. A.; Ces, O.; French, P.; Willison, K. R.; Klug, D. *Lab Chip* **2011**, *11*, 1256−1261.
(10) Ko, S. H.; Kim, S. J.; Cheow, L. F.; Li, L. D.; Kang, K. H.; Han, J. *Lab Chip* **2011**, *11*, 1351−1358.
(11) Mir, M.; Homs, A.; Samitier, J. *Electrophoresis* **2009**, *30*, 3386−3397.
(12) Foote, R. S.; Khandurina, J.; Jacobson, S. C.; Ramsey, J. M. *Anal. Chem.* **2005**, *77*, 57−63.
(13) Khandurina, J.; Jacobson, S. C.; Waters, L. C.; Foote, R. S.; Ramsey, J. M. *Anal. Chem.* **1999**, *71*, 1815−1819.
(14) Ramsey, J. D.; Collins, G. E. *Anal. Chem.* **2005**, *77*, 6664−6670.
(15) Chang, W.; Komazu, T.; Korenaga, T. *Anal. Lett.* **2008**, *41*, 1468−1476.
(16) Hofmann, O.; Che, D. P.; Cruickshank, K. A.; Muller, U. R. *Anal. Chem.* **1999**, *71*, 678−686.
(17) Macounova, K.; Cabrera, C. R.; Holl, M. R.; Yager, P. *Anal. Chem.* **2000**, *72*, 3745−3751.
(18) Wen, J.; Wilker, E. W.; Yaffe, M. B.; Jensen, K. F. *Anal. Chem.* **2010**, *82*, 1253−1260.
(19) Tang, G. Y.; Yang, C. *Electrophoresis* **2008**, *29*, 1006−1012.
(20) Ge, Z. W.; Wang, W.; Yang, C. *Lab Chip* **2011**, *11*, 1396−1402.
(21) Wang, Y. C.; Stevens, A. L.; Han, J. Y. *Anal. Chem.* **2005**, *77*, 4293−4299.
(22) Chun, H. G.; Chung, T. D.; Ramsey, J. M. *Anal. Chem.* **2010**, *82*, 6287−6292.
(23) Shen, M.; Yang, H.; Sivagnanam, V.; Gijs, M. A. M. *Anal. Chem.* **2010**, *82*, 9989−9997.
(24) Humble, P. H.; Kelly, R. T.; Woolley, A. T.; Tolley, H. D.; Lee, M. L. *Anal. Chem.* **2004**, *76*, 5641−5648.
(25) Petsev, D. N.; Lopez, G. P.; Ivory, C. F.; Sibbett, S. S. *Lab Chip* **2005**, *5*, 587−597.
(26) Koegler, W. S.; Ivory, C. F. *J. Chromatogr., A* **1996**, *726*, 229−236.
(27) Burke, J. M.; Ivory, C. F. *Electrophoresis* **2010**, *31*, 893−901.
(28) Kelly, R. T.; Woolley, A. T. *J. Sep. Sci.* **2005**, *28*, 1985−1993.
(29) Burke, J. M.; Huang, Z.; Ivory, C. F. *Anal. Chem.* **2009**, *81*, 8236−8243.
(30) McDonald, J. C.; Duffy, D. C.; Anderson, J. R.; Chiu, D. T.; Wu, H. K.; Schueller, O. J. A.; Whitesides, G. M. *Electrophoresis* **2000**, *21*, 27−40.
(31) Liu, X. Z.; Erickson, D.; Li, D. Q.; Krull, U. J. *Anal. Chim. Acta* **2004**, *507*, 55−62.
(32) Spehar, A. M.; Koster, S.; Linder, V.; Kulmala, S.; de Rooij, N. F.; Verpoorte, E.; Sigrist, H.; Thormann, W. *Electrophoresis* **2003**, *24*, 3674−3678.
(33) Boonsong, K.; Caulum, M. M.; Dressen, B. M.; Chailapakul, O.; Cropek, D. M.; Henry, C. S. *Electrophoresis* **2008**, *29*, 3128−3134.
(34) Anand, R. K.; Sheridan, E.; Hlushkou, D.; Tallarek, U.; Crooks, R. M. *Lab Chip* **2011**, *11*, 518−527.
(35) Knust, K. N.; Sheridan, E.; Anand, R. K.; Crooks, R. M. *Lab Chip* **2012**, in press, DOI: 10.1039/C2LC40660H.